

RESEARCH ARTICLE

[View Article Online](#)  
[View Journal](#) | [View Issue](#)



Cite this: *Inorg. Chem. Front.*, 2023, **10**, 1431

## High-efficiency electrosynthesis of ammonia with selective reduction of nitrite over an Ag nanoparticle-decorated $\text{TiO}_2$ nanoribbon array<sup>†</sup>

Xiaoya Fan,<sup>a,b</sup> Xun He,<sup>b</sup> Xianchang Ji,<sup>b</sup> Longcheng Zhang,<sup>b</sup> Jun Li,<sup>b</sup> Long Hu,<sup>b</sup> XiuHong Li,<sup>b</sup> Shengjun Sun,<sup>c</sup> Dongdong Zheng,<sup>b</sup> Yongsong Luo,<sup>b</sup> Yan Wang,<sup>b</sup> Lisi Xie,<sup>d</sup> Qian Liu,<sup>d</sup> Binwu Ying<sup>b,\*a</sup> and Xuping Sun<sup>b,\*b,c</sup>

Electrochemical nitrite ( $\text{NO}_2^-$ ) reduction can yield value-added ammonia ( $\text{NH}_3$ ) while removing  $\text{NO}_2^-$  as an environmental pollutant in wastewater; however, it involves a six-electron transfer process and requires highly efficient and selective electrocatalysts. In this study, we report high-efficiency electrosynthesis of  $\text{NH}_3$  via  $\text{NO}_2^-$  reduction enabled by an Ag nanoparticle-decorated  $\text{TiO}_2$  nanoribbon array on a titanium plate (Ag@ $\text{TiO}_2$ /TP). When tested in 0.1 M NaOH containing 0.1 M  $\text{NO}_2^-$ , such Ag@ $\text{TiO}_2$ /TP shows a large  $\text{NH}_3$  yield of 514.3  $\mu\text{mol h}^{-1} \text{cm}^{-2}$  and a high faradaic efficiency of 96.4% at  $-0.5$  V vs. a reversible hydrogen electrode. Significantly, it also demonstrates excellent durability for 12 h electrolysis.

Received 14th November 2022,  
Accepted 11th January 2023

DOI: 10.1039/d2qi02409h  
[rsc.li/frontiers-inorganic](http://rsc.li/frontiers-inorganic)

Ammonia ( $\text{NH}_3$ ) is widely applied to manufacture nitrogen fertilizers, explosives, chemical products, *etc.*, and it is also considered as an attractive hydrogen carrier and zero-carbon fuel.<sup>1–3</sup> Although the Haber–Bosch method realizes industrial  $\text{NH}_3$  synthesis from hydrogen and nitrogen under high temperature and high pressure, this process is highly energy-intensive and emits a mass of greenhouse gases.<sup>4</sup> Electrochemical nitrogen reduction is thus deemed as a potential alternative to the Haber–Bosch process for ambient  $\text{NH}_3$  synthesis, although the competitive hydrogen evolution reaction and unsatisfactory adsorption and cleavage effects of  $\text{N}_2$  severely hinder the selectivity and activity of the electrochemical nitrogen reduction reaction.<sup>5–14</sup>

$\text{NH}_3$  synthesis *via* electrochemical nitrite ( $\text{NO}_2^-$ ) reduction, in contrast, needs lower energy to cleave the  $\text{N}=\text{O}$  bond with faster reaction kinetics and achieves higher reaction substrate concentrations, leading to a larger  $\text{NH}_3$  yield and higher faradaic efficiency (FE).<sup>1,15,16</sup> In addition, excess  $\text{NO}_2^-$  accumulated in groundwater could destroy the ecological balance and harm human health.<sup>17</sup> Electrochemical conversion of waste  $\text{NO}_2^-$  can produce value-added  $\text{NH}_3$  under ambient conditions

and simultaneously remove  $\text{NO}_2^-$ , which provides a solution for restoring the imbalance in the global nitrogen cycle. However, the electrochemical  $\text{NO}_2^-$  reduction reaction ( $\text{NO}_2^-$ RR) involves a complex six-electron pathway with various possible by-products ( $\text{N}_2\text{H}_4$ ,  $\text{N}_2$ , and  $\text{H}_2$ ), thus requiring highly active catalysts for selective  $\text{NO}_2^-$ -to- $\text{NH}_3$  conversion.<sup>18–27</sup>

Noble metal (Au,<sup>28</sup> Pd,<sup>28,29</sup> Ru,<sup>30</sup> Ir,<sup>31</sup> Pt<sup>32</sup>)-based catalysts are active for the  $\text{NO}_2^-$ RR, but their scarcity hinders large-scale applications. Compared with the above noble metals, Ag is relatively low in price and high in abundance, and it also performs efficiently in  $\text{NO}_2^-$  reduction electrocatalysis.<sup>33</sup> As an Earth-abundant transition metal oxide with high chemical and structural stability,  $\text{TiO}_2$  is widely used as a support to load noble metal nanoparticles for catalysis applications.<sup>34–39</sup> Our recent studies also suggest that it is active for the  $\text{NO}_2^-$ RR and its activity can be enhanced by introducing oxygen vacancies<sup>40</sup> and P doping.<sup>41</sup> We believe that  $\text{TiO}_2$  could be an ideal support for Ag nanoparticles for an enhanced  $\text{NO}_2^-$ -to- $\text{NH}_3$  conversion performance with much less usage of noble metals, which, however, has not been reported to date.

In this study, we constructed an Ag nanoparticle-decorated  $\text{TiO}_2$  nanoribbon array on a titanium plate (Ag@ $\text{TiO}_2$ /TP) as a highly selective  $\text{NO}_2^-$ RR catalyst for  $\text{NH}_3$  synthesis. When tested in  $\text{NO}_2^-$ -containing solution, Ag@ $\text{TiO}_2$ /TP is capable of delivering a large  $\text{NH}_3$  yield of 514.3  $\mu\text{mol h}^{-1} \text{cm}^{-2}$  with a high FE of 96.4% at  $-0.5$  V *vs.* a reversible hydrogen electrode (RHE). Furthermore, Ag@ $\text{TiO}_2$ /TP exhibits robust stability for long-term electrolysis.

As shown in Fig. 1a, Ag@ $\text{TiO}_2$ /TP was synthesized through a hydrothermal method in an alkaline solution,  $\text{Ag}^+$  exchange,

<sup>a</sup>Department of Laboratory Medicine, West China Hospital, Sichuan University, Chengdu 610041, Sichuan, China. E-mail: [yingbinwu@scu.edu.cn](mailto:yingbinwu@scu.edu.cn)

<sup>b</sup>Institute of Fundamental and Frontier Sciences, University of Electronic Science and Technology of China, Chengdu 610054, Sichuan, China. E-mail: [xpsun@uestc.edu.cn](mailto:xpsun@uestc.edu.cn), [xpsun@sdu.edu.cn](mailto:xpsun@sdu.edu.cn)

<sup>c</sup>College of Chemistry, Chemical Engineering and Materials Science, Shandong Normal University, Jinan 250014, Shandong, China

<sup>d</sup>Institute for Advanced Study, Chengdu University, Chengdu 610068, Sichuan, China

<sup>†</sup>Electronic supplementary information (ESI) available: Experimental section and supplementary figures. See DOI: <https://doi.org/10.1039/d2qi02409h>

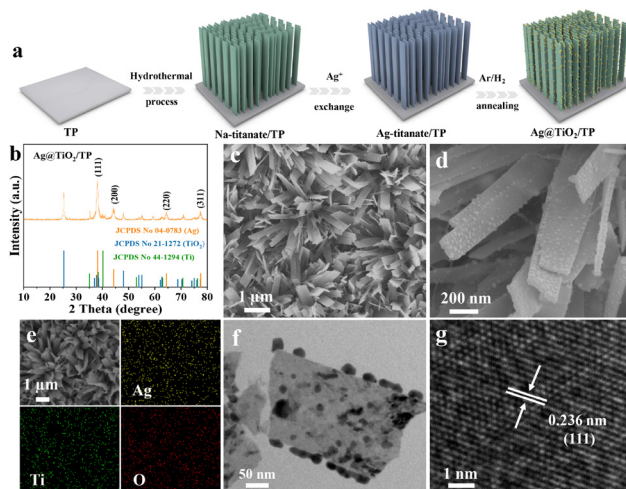


**Fig. 1** (a) Schematic illustration of the fabrication process of Ag@TiO<sub>2</sub>/TP. (b) XRD pattern and (c) and (d) SEM images of Ag@TiO<sub>2</sub>/TP. (e) SEM and corresponding elemental mapping images of Ag@TiO<sub>2</sub>/TP. (f) TEM and (g) HRTEM images of Ag@TiO<sub>2</sub>.

and an annealing process under an Ar/H<sub>2</sub> atmosphere (see the ESI† for details). Fig. 1b depicts the X-ray diffraction (XRD) pattern of Ag@TiO<sub>2</sub>/TP. The diffraction peaks at 38.15°, 44.30°, 64.43°, and 77.50° correspond to the (111), (200), (220), and (311) lattice planes of Ag, respectively (JCPDS No. 04-0783),<sup>33</sup> while the other diffraction peaks can be assigned to metallic Ti (JCPDS No. 44-1294) and TiO<sub>2</sub> (JCPDS No. 21-1272), and these are in accordance with those for TiO<sub>2</sub>/TP (Fig. S1†). As depicted in Fig. S2 and S3,† the scanning electron microscopy (SEM) images show that the TiO<sub>2</sub> nanoribbon array was grown on TP. With regard to Ag@TiO<sub>2</sub>/TP, plenty of nanoparticles are decorated on the surface of the TiO<sub>2</sub> nanoribbon (Fig. 1c and d). Additionally, the SEM image and corresponding energy-dispersive X-ray (EDX) elemental mapping images of Ag@TiO<sub>2</sub>/TP confirm the existence of Ag, Ti, and O elements with a homogeneous distribution (Fig. 1e). Furthermore, the result of the EDX spectrum confirms that the Ag content in Ag@TiO<sub>2</sub>/TP is approximately 13.63% (Fig. S4†). The transmission electron microscopy (TEM) image also provides evidence of the formation of a large number of nanoparticles without agglomeration on the nanoribbon, as shown in Fig. 1f. A high-resolution TEM (HRTEM) image taken from one such nanoparticle displays a lattice spacing of 0.236 nm indexed to the (111) plane of Ag (Fig. 1g). All these observations confirm the successful fabrication of an Ag nanoparticle-decorated TiO<sub>2</sub> nanoribbon array.

The X-ray photoelectron spectroscopy (XPS) survey spectrum (Fig. 2a) also shows the presence of Ag, O, and Ti elements. The Ag 3d region spectrum (Fig. 2b) is divided into two peaks at 368.28 and 374.28 eV, which are ascribed to Ag 3d<sub>5/2</sub> and Ag 3d<sub>3/2</sub>, respectively.<sup>42,43</sup> In the Ti 2p spectrum, two fitting peaks at 459.38 and 465.08 eV are assigned to Ti 2p<sub>3/2</sub> and Ti 2p<sub>1/2</sub>, respectively (Fig. 2c).<sup>44,45</sup> In addition, two fitting peaks in the O 1s spectrum are attributed to metal–oxygen bonds (M–O,

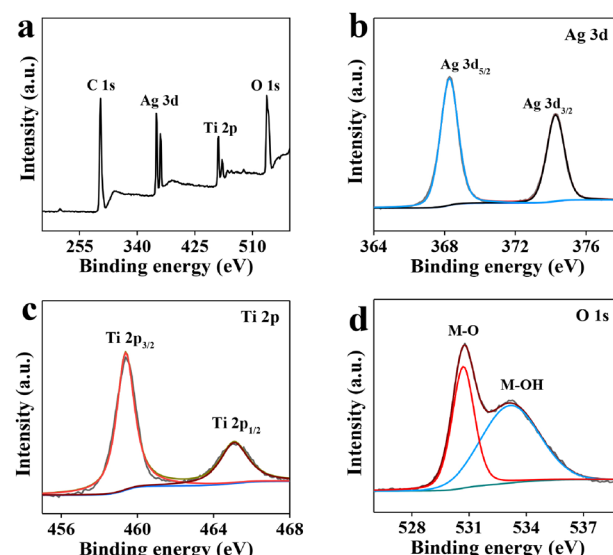


**Fig. 2** (a) XPS survey spectrum, and high resolution XPS spectra in the (b) Ag 3d, (c) Ti 2p, and (d) O 1s regions of Ag@TiO<sub>2</sub>.

530.78 eV) and adsorbed surface hydroxyl groups (M–OH, 533.18 eV) (Fig. 2d).<sup>42,45</sup>

The electrochemical experiments of Ag@TiO<sub>2</sub>/TP, Ag/TP, and TiO<sub>2</sub>/TP toward the NO<sub>2</sub><sup>−</sup>RR were implemented in Ar-saturated NO<sub>2</sub><sup>−</sup>-free and NO<sub>2</sub><sup>−</sup>-containing 0.1 M NaOH electrolytes. UV-vis spectra and related calibration curves are depicted in Fig. S5 and S6.† Linear scanning voltammetry (LSV) of Ag@TiO<sub>2</sub>/TP was firstly conducted. Obviously, a markedly enhanced current density (*j*) emerges upon the addition of NO<sub>2</sub><sup>−</sup> (Fig. 3a), verifying that Ag@TiO<sub>2</sub>/TP enables efficient NO<sub>2</sub><sup>−</sup> reduction. In comparison, Ag/TP and TiO<sub>2</sub>/TP display lower *j* with NO<sub>2</sub><sup>−</sup>-containing electrolytes (Fig. S7†), confirming that the electrocatalytic NO<sub>2</sub><sup>−</sup>RR activity of Ag@TiO<sub>2</sub>/TP is superior to those of Ag/TP

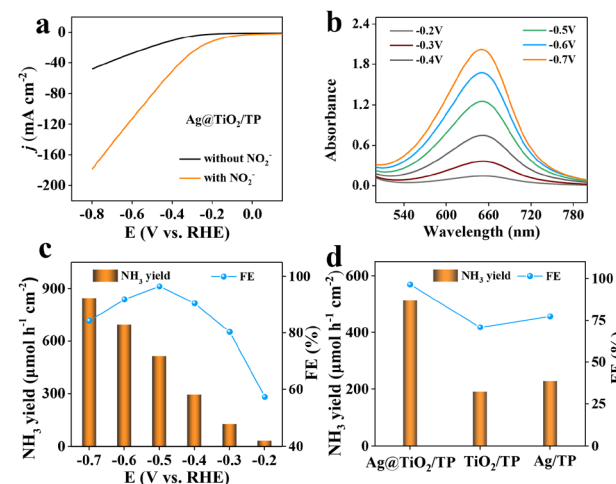


**Fig. 3** (a) LSV curves of Ag@TiO<sub>2</sub>/TP in 0.1 M NaOH with/without 0.1 M NO<sub>2</sub><sup>−</sup>. (b) UV-vis spectra of Ag@TiO<sub>2</sub>/TP at various potentials. (c) NH<sub>3</sub> yields and FEs of Ag@TiO<sub>2</sub>/TP at various potentials. (d) Comparison of NH<sub>3</sub> yields and FEs of Ag@TiO<sub>2</sub>/TP, TiO<sub>2</sub>/TP, and Ag/TP at -0.5 V.

and  $\text{TiO}_2/\text{TP}$ . Chronoamperometry (CA) measurements at given potentials (from  $-0.2$  V to  $-0.7$  V) were then executed to study the  $\text{NH}_3$ -generation ability of  $\text{Ag@TiO}_2/\text{TP}$  (Fig. S8†), where the peak intensity of the relevant UV-vis spectra strengthens with an increase in the given potential (Fig. 3b), manifesting that a more negative potential results in more  $\text{NH}_3$ . Furthermore, we evaluated  $\text{NH}_3$  FEs and yields of  $\text{Ag@TiO}_2/\text{TP}$  in test windows (Fig. 3c). Noticeably, as the cathode potential negatively shifts, the  $\text{NH}_3$  yields of  $\text{Ag@TiO}_2/\text{TP}$  progressively increase, and eventually the largest value of  $846.3 \mu\text{mol h}^{-1} \text{cm}^{-2}$  ( $14\,387.1 \mu\text{g h}^{-1} \text{cm}^{-2}$ ) at  $-0.7$  V is obtained. Furthermore, the maximum FE of  $\text{NH}_3$  production is 96.4% at  $-0.5$  V with an  $\text{NH}_3$  yield of  $514.3 \mu\text{mol h}^{-1} \text{cm}^{-2}$  ( $8743.1 \mu\text{g h}^{-1} \text{cm}^{-2}$ ), confirming an excellent  $\text{NO}_2^-$ RR electrocatalyst. The  $\text{NH}_3$  yields and FEs of  $\text{Ag@TiO}_2/\text{TP}$  exceed those of most reported  $\text{NO}_2^-$ RR electrocatalysts (Table S1†). As shown in Fig. 3d,  $\text{Ag@TiO}_2/\text{TP}$  exhibits a much better performance than  $\text{Ag/TP}$  (77.38%,  $228.5 \mu\text{mol h}^{-1} \text{cm}^{-2}$ ) and  $\text{TiO}_2/\text{TP}$  (70.8%,  $190.9 \mu\text{mol h}^{-1} \text{cm}^{-2}$ ).

The  $\text{NO}_2^-$  reduction process of  $\text{Ag@TiO}_2/\text{TP}$  was further assessed by quantifying various by-products ( $\text{N}_2\text{H}_4$ ,  $\text{H}_2$ , and  $\text{N}_2$ ). As exhibited in Fig. S9,† no  $\text{N}_2\text{H}_4$  signals were monitored as was proved by identical UV-vis absorption spectral peaks at different potentials. Meanwhile, traces of  $\text{H}_2$  and  $\text{N}_2$  were detected (Fig. 4a) with the maximal  $\text{H}_2$  and  $\text{N}_2$  yields being  $2.82 \mu\text{mol h}^{-1} \text{cm}^{-2}$  and  $1.85 \mu\text{mol h}^{-1} \text{cm}^{-2}$ , with FEs of 4.9% and 1.42%, respectively, much lower than that of  $\text{NH}_3$  at every

potential, verifying the superb selectivity of such  $\text{Ag@TiO}_2/\text{TP}$  electrocatalysts for  $\text{NH}_3$  synthesis. Furthermore, the partial current densities ( $j_{\text{partial}}$ ) of  $\text{Ag@TiO}_2/\text{TP}$  for  $\text{NH}_3$  reach  $-122.1 \text{ mA cm}^{-2}$  at  $-0.7$  V, clearly higher than that of  $\text{H}_2$  ( $-4.1 \text{ mA cm}^{-2}$ ) and  $\text{N}_2$  ( $-1.04 \text{ mA cm}^{-2}$ ) (Fig. 4b), again proving great  $\text{NO}_2^-$ RR selectivity towards  $\text{NH}_3$  electrosynthesis. Control experiments were then performed to determine whether the synthesized  $\text{NH}_3$  just comes from the  $\text{NO}_2^-$ RR on  $\text{Ag@TiO}_2/\text{TP}$ . It is clearly seen that the amounts of  $\text{NH}_3$  generated after 1 h of electrolysis in a blank solution ( $0.29 \mu\text{g}$ ) and open circuit potential (OCP,  $0.66 \mu\text{g}$ ) are extremely small (Fig. S10†), which excludes possible interference factors from the electrolytic solution and device.

Six alternative-cycle measurements were then carried out in  $\text{NO}_2^-$ -free/ $\text{NO}_2^-$ -containing electrolytes at  $-0.5$  V, and  $\text{NH}_3$  only is generated in  $\text{NO}_2^-$ -containing electrolytes (Fig. 4c), demonstrating that  $\text{NH}_3$  just originates from  $\text{NO}_2^-$  via the  $\text{NO}_2^-$ RR on  $\text{Ag@TiO}_2/\text{TP}$ . Additionally, stability is an extremely important parameter of the  $\text{NO}_2^-$ RR process for  $\text{NH}_3$  synthesis. We thus implemented a 12 h electrolysis test, as displayed in Fig. 4d, and the  $\text{Ag@TiO}_2/\text{TP}$  electrode maintained an initial  $j$  of nearly 100% with almost no fluctuation, confirming the excellent tolerance of our catalyst. Furthermore, we carried out 8 consecutive measurements on  $\text{Ag@TiO}_2/\text{TP}$  at  $-0.5$  V, and the volatility of  $\text{NH}_3$  yields and FEs was negligible, again proving the durability of  $\text{Ag@TiO}_2/\text{TP}$  (Fig. 4e and S11†), which is also in good accordance with the LSV curve (Fig. S12†), XRD pattern (Fig. S13†), and SEM images (Fig. S14†) of  $\text{Ag@TiO}_2/\text{TP}$  after long-term electrolysis. These results suggest that  $\text{Ag@TiO}_2/\text{TP}$  has excellent stability for the electrocatalytic reduction of  $\text{NO}_2^-$  to  $\text{NH}_3$ .

In summary, a  $\text{Ag}$  nanoparticle-decorated  $\text{TiO}_2$  nanoribbon array is proved to be an efficient and stable  $\text{NO}_2^-$ RR catalyst for  $\text{NO}_2^-$ -to- $\text{NH}_3$  conversion in an alkaline electrolyte, producing a remarkable  $\text{NH}_3$  yield of  $8743.1 \mu\text{g h}^{-1} \text{cm}^{-2}$  with a large FE of 96.4%. This study not only offers a highly selective electrocatalyst for ambient  $\text{NH}_3$  synthesis via  $\text{NO}_2^-$  reduction, but also opens up a new avenue to construct a nanostructured  $\text{Ag/TiO}_2$  hybrid array for applications.

## Conflicts of interest

There are no conflicts to declare.

## Acknowledgements

This work was supported by the National Natural Science Foundation of China (No. 22072015).

## References

- 1 J. Liang, Q. Liu, A. A. Alshehri and X. Sun, Recent advances in nanostructured heterogeneous catalysts for N-cycle electrocatalysis, *Nano Res. Energy*, 2022, **1**, e9120010.

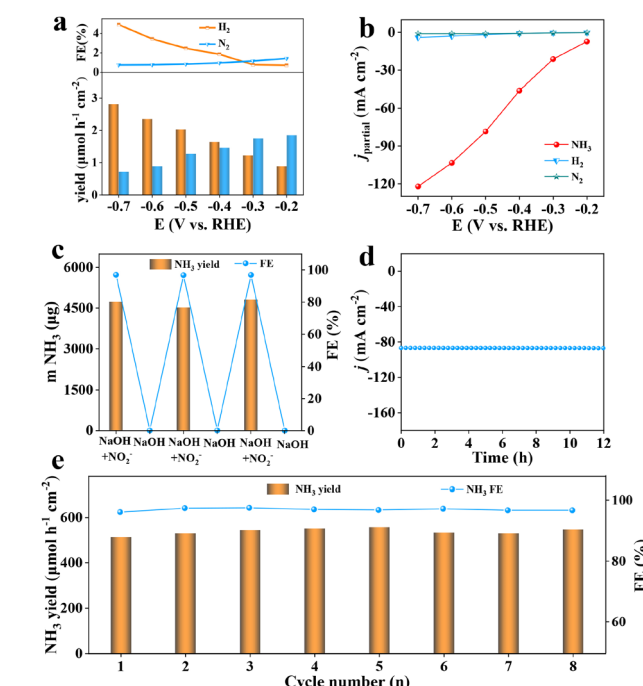


**Fig. 4** (a) Yields and FEs of  $\text{N}_2$  and  $\text{H}_2$  of  $\text{Ag@TiO}_2/\text{TP}$  at different potentials. (b)  $j_{\text{partial}}$  of  $\text{NH}_3$ ,  $\text{N}_2$ , and  $\text{H}_2$  of  $\text{Ag@TiO}_2/\text{TP}$  at different potentials. (c)  $\text{NH}_3$  yields and FEs of  $\text{Ag@TiO}_2/\text{TP}$  during the alternating cycling tests. (d) Time-dependent current density curve during 12 h electrolysis of  $\text{Ag@TiO}_2/\text{TP}$  at  $-0.5$  V. (e) Recycling tests of  $\text{Ag@TiO}_2/\text{TP}$  at  $-0.5$  V.

2 J. Liang, W. Hu, B. Song, T. Mou, L. Zhang, Y. Luo, Q. Liu, A. A. Alshehri, M. S. Hamdy, L. Yang and X. Sun, Efficient nitric oxide electroreduction toward ambient ammonia synthesis catalyzed by a CoP nanoarray, *Inorg. Chem. Front.*, 2022, **9**, 1366–1372.

3 D. Qi, F. Lv, T. Wei, M. Jin, G. Meng, S. Zhang, Q. Liu, W. Liu, D. Ma, M. S. Hamdy, J. Luo and X. Liu, High-efficiency electrocatalytic NO reduction to NH<sub>3</sub> by nanoporous VN, *Nano Res. Energy*, 2022, **1**, e9120022.

4 I. Dybkaer, in *Ammonia, catalysis and manufacture*, ed. A. Nielsen, Springer, Heidelberg, 1995, pp. 199–327.

5 Y. Ji, L. Li, W. Cheng, Y. Xiao, C. Li and X. Liu, A CeP nanoparticle-reduced graphene oxide hybrid: an efficient electrocatalyst for the NH<sub>3</sub> synthesis under ambient conditions, *Inorg. Chem. Front.*, 2021, **8**, 2103–2106.

6 L. Li, C. Tang, H. Jin, K. Davey and S.-Z. Qiao, Main-group elements boost electrochemical nitrogen fixation, *Chem.*, 2021, **7**, 3232–3255.

7 N. Cao, Z. Chen, K. Zang, J. Xu, J. Zhong, J. Luo, X. Xu and G. Zheng, Doping strain induced Bi-Ti<sup>3+</sup> pairs for efficient N<sub>2</sub> activation and electrocatalytic fixation, *Nat. Commun.*, 2019, **10**, 2877.

8 C. Guo, J. Ran, A. Vasileff and S. Qiao, Rational design of electrocatalysts and photo(electro)catalysts for nitrogen reduction to ammonia (NH<sub>3</sub>) under ambient conditions, *Energy Environ. Sci.*, 2018, **11**, 45–56.

9 D. Chanda, R. Xing, T. Xu, Q. Liu, Y. Luo, S. Liu, R. A. Tufa, T. H. Dolla, T. Montini and X. Sun, Electrochemical nitrogen reduction: recent progress and prospects, *Chem. Commun.*, 2021, **57**, 7335–7349.

10 Y. Luo, Q. Li, Y. Tian, Y. Liu and K. Chu, Amorphization engineered VSe<sub>2-x</sub> nanosheets with abundant Se-vacancies for enhanced N<sub>2</sub> electroreduction, *J. Mater. Chem. A*, 2022, **10**, 1742–1749.

11 Y. Li, Y. Liu, J. Wang, Y. Guo and K. Chu, Plasma-engineered NiO nanosheets with enriched oxygen vacancies for enhanced electrocatalytic nitrogen fixation, *Inorg. Chem. Front.*, 2020, **7**, 455–463.

12 S. Zhang, C. Zhao, Y. Liu, W. Li, J. Wang, G. Wang, Y. Zhang, H. Zhang and H. Zhao, Cu doping in CeO<sub>2</sub> to form multiple oxygen vacancies for dramatically enhanced ambient N<sub>2</sub> reduction performance, *Chem. Commun.*, 2019, **55**, 2952–2955.

13 C. Liu, S. Li, Z. Li, L. Zhang, H. Chen, D. Zhao, S. Sun, Y. Luo, A. A. Alshehri, M. S. Hamdy, Q. Liu and X. Sun, Ambient N<sub>2</sub>-to-NH<sub>3</sub> fixation over CeO<sub>2</sub> nanoparticles decorated three-dimensional carbon skeleton, *Sustainable Energy Fuels*, 2022, **6**, 3344–3348.

14 Q. Li, P. Shen, Y. Tian, X. Li and K. Chu, Metal-free BN quantum dots/graphitic C<sub>3</sub>N<sub>4</sub> heterostructure for nitrogen reduction reaction, *J. Colloid Interface Sci.*, 2022, **606**, 204–212.

15 X. He, X. Li, X. Fan, J. Li, D. Zhao, L. Zhang, S. Sun, Y. Luo, D. Zheng, L. Xie, A. M. Asiri, Q. Liu and X. Sun, Ambient electroreduction of nitrite to ammonia over Ni nanoparticle supported on molasses-derived carbon sheets, *ACS Appl. Nano Mater.*, 2022, **5**, 14246–14250.

16 S. Li, J. Liang, P. Wei, Q. Liu, L. Xie, Y. Luo and X. Sun, ITO@TiO<sub>2</sub> nanoarray: an efficient and robust NO<sub>2</sub><sup>-</sup> reduction reaction electrocatalyst toward NH<sub>3</sub> production under ambient conditions, *eScience*, 2022, **2**, 382–388.

17 X. Zhu, X. Zeng, X. Chen, W. Wu and Y. Wang, Inhibitory effect of nitrate/nitrite on the microbial reductive dissolution of arsenic and iron from soils into pore water, *Ecotoxicology*, 2019, **28**, 528–538.

18 Q. Liu, Q. Liu, X. Lisi, L. Yue, T. Li, Y. Luo, N. Li, B. Tang, L. Yu and X. Sun, 3D FeOOH nanotube array: an efficient catalyst for ammonia electrosynthesis by nitrite reduction, *Chem. Commun.*, 2022, **58**, 5160–5163.

19 C. Wang, W. Zhou, Z. Sun, Y. Wang, B. Zhang and Y. Yu, Integrated selective nitrite reduction to ammonia with tetrahydroisoquinoline semi-dehydrogenation over a vacancy-rich Ni bifunctional electrode, *J. Mater. Chem. A*, 2021, **9**, 239–243.

20 L. Hu, D. Zhao, C. Liu, Y. Liang, D. Zheng, S. Sun, Q. Li, Q. Liu, Y. Luo, Y. Liao, L. Xie and X. Sun, Amorphous CoB nanoarray as a high-efficiency electrocatalyst for nitrite reduction to ammonia, *Inorg. Chem. Front.*, 2022, **9**, 6075–6079.

21 X. Zhang, Y. Wang, Y. Wang, Y. Guo, X. Xie, Y. Yu and B. Zhang, Recent advances in electrocatalytic nitrite reduction, *Chem. Commun.*, 2022, **58**, 2777–2787.

22 L. Ouyang, L. Yue, Q. Liu, Q. Liu, Z. Li, S. Sun, Y. Luo, A. A. Alshehri, M. S. Hamdy, Q. Kong and X. Sun, Cu nanoparticles decorated juncus-derived carbon for efficient electrocatalytic nitrite-to-ammonia conversion, *J. Colloid Interface Sci.*, 2022, **624**, 394–399.

23 J. Wang, T. Feng, J. Chen, V. Ramalingam, Z. Li, D. M. Kabtamu, J. He and X. Fang, Electrocatalytic nitrate/nitrite reduction to ammonia synthesis using metal nanocatalysts and bio-inspired metalloenzymes, *Nano Energy*, 2021, **86**, 106088.

24 L. Mattarozzi, S. Cattarina, N. Comissoa, P. Guerriero, M. Musiani, L. Vázquez-Gómez and E. Verlatoa, Electrochemical reduction of nitrate and nitrite in alkaline media at CuNi alloy electrodes, *Electrochim. Acta*, 2013, **89**, 488–496.

25 R. Zhang, S. Zhang, Y. Guo, C. Li, J. Liu, Z. Huang, Y. Zhao, Y. Li and C. Zhi, A Zn-nitrite battery as an energy-output electrocatalytic system for high-efficiency ammonia synthesis using carbon-doped cobalt oxide nanotubes, *Energy Environ. Sci.*, 2022, **15**, 3024–3032.

26 S. E. Braley, J. Xie, Y. Losovjy and J. M. Smith, Graphite conjugation of a macrocyclic cobalt complex enhances nitrite electroreduction to ammonia, *J. Am. Chem. Soc.*, 2021, **143**, 7203–7208.

27 Z. Chen, A. Jaworski, J. Chen, T. M. Budnyak, I. Szewczyk, A. Rokicińska, R. Dronkowski, N. Hedin, P. Kuśtrowski and A. Slabon, Graphitic nitrogen in carbon catalysts is important for the reduction of nitrite as revealed by naturally abundant <sup>15</sup>N NMR spectroscopy, *Dalton Trans.*, 2021, **50**, 6857–6866.

28 H. Li, S. Guo, K. Shin, M. S. Wong and G. Henkelman, Design of a Pd–Au nitrite reduction catalyst by identifying and optimizing active ensembles, *ACS Catal.*, 2019, **9**, 7957–7966.

29 H. Shin, S. Jung, S. Bae, W. Lee and H. Kim, Nitrite reduction mechanism on a Pd surface, *Environ. Sci. Technol.*, 2014, **48**, 12768–12774.

30 X. Huo, D. J. Van Hoomissen, J. Liu, S. Vyas and T. J. Strathmann, Hydrogenation of aqueous nitrate and nitrite with ruthenium catalysts, *Appl. Catal., B*, 2017, **211**, 188–198.

31 H. Li, C. Yan, H. Guo, K. Shin, S. M. Humphrey, C. J. Werth and G. Henkelman,  $\text{Cu}_x\text{Ir}_{1-x}$  nanoalloy catalysts achieve near 100% selectivity for aqueous nitrite reduction to  $\text{NH}_3$ , *ACS Catal.*, 2020, **10**, 7915–7921.

32 M. C. Figueiredo, V. Climent and J. M. Feliu, Nitrite reduction on bismuth modified Pt (111) surfaces in different electrolytic media, *Electrocatalysis*, 2011, **2**, 255–262.

33 Q. Liu, G. Wen, D. Zhao, L. Xie, S. Sun, L. Zhang, Y. Luo, A. A. Alshehri, M. S. Hamdy, Q. Kong and X. Sun, Nitrite reduction over Ag nanoarray electrocatalyst for ammonia synthesis, *J. Colloid Interface Sci.*, 2022, **623**, 513–519.

34 S. Chang and X. Xu, Au nanocrystals decorated  $\text{TiO}_2$  nanotubes for photocatalytic nitrogen fixation into ammonia, *Inorg. Chem. Front.*, 2020, **7**, 620–624.

35 W. Shi, A.-H. Park, S. Xu, P. J. Yoo and Y.-U. Kwon, Continuous and conformal thin  $\text{TiO}_2$ -coating on carbon support makes Pd nanoparticles highly efficient and durable electrocatalyst, *Appl. Catal., B*, 2021, **284**, 119715.

36 A. Shoaib, M. Ji, H. Qian, J. Liu, M. Xu and J. Zhang, Noble metal nanoclusters and their in situ calcination to nanocrystals: precise control of their size and interface with  $\text{TiO}_2$  nanosheets and their versatile catalysis applications, *Nano Res.*, 2016, **9**, 1763–1774.

37 S. Zhang, W. Wang, Y. Gao, S. Deng, L. Ding, H. Zhuo, Z. Bao, W. Ji, C. Qiu and J. Wang, Pd–Co alloy supported on  $\text{TiO}_2$  with oxygen vacancies for efficient  $\text{N}_2$  and  $\text{O}_2$  electrocatalytic reduction, *Appl. Surf. Sci.*, 2021, **567**, 150680.

38 L.-N. Chen, S.-H. Wang, P.-Y. Zhang, Z.-X. Chen, L. Xiao, H.-J. Yang, T. Sheng, W.-F. Lin, N. Tian, S.-G. Sun and Z.-Y. Zhou, Ru nanoparticles supported on partially reduced  $\text{TiO}_2$  as highly efficient catalyst for hydrogen evolution, *Nano Energy*, 2021, **88**, 106211.

39 Z.-W. Wei, H.-J. Wang, C. Zhang, K. Xu, X.-L. Lu and T.-B. Lu, Reversed charge transfer and enhanced hydrogen spillover in platinum nanoclusters anchored on titanium oxide with rich oxygen vacancies boost hydrogen evolution reaction, *Angew. Chem., Int. Ed.*, 2021, **60**, 16622–16627.

40 D. Zhao, J. Liang, J. Li, L. Zhang, K. Dong, L. Yue, Y. Luo, Y. Ren, Q. Liu, M. S. Hamdy, Q. Kong, Q. Liu and X. Sun, A  $\text{TiO}_{2-x}$  nanobelt array with oxygen vacancies: an efficient electrocatalyst toward nitrite conversion to ammonia, *Chem. Commun.*, 2022, **58**, 3669–3672.

41 L. Ouyang, X. He, S. Sun, Y. Luo, D. Zheng, J. Chen, Y. Li, Y. Lin, Q. Liu, A. M. Asirif and X. Sun, Enhanced electrocatalytic nitrite reduction to ammonia over P-doped  $\text{TiO}_2$  nanobelt array, *J. Mater. Chem. A*, 2022, **10**, 23494–23498.

42 Q. Qin, Y. Li, W. Bu, L. Meng, X. Chuai, Z. Zhou and C. Hu, Self-template-derived  $\text{ZnCo}_2\text{O}_4$  porous microspheres decorated by Ag nanoparticles and their selective detection of formaldehyde, *Inorg. Chem. Front.*, 2021, **8**, 811–820.

43 Y. Fang, S. Zhang, Z.-P. Wu, D. Luan and X. W. Lou, A highly stable lithium metal anode enabled by Ag nanoparticle-embedded nitrogen-doped carbon macroporous fibers, *Sci. Adv.*, 2021, **7**, eabg3626.

44 Y. Guo, R. Zhang, S. Zhang, Y. Zhao, Q. Yang, Z. Huang, B. Dong and C. Zhi, Pd doping-weakened intermediate adsorption to promote electrocatalytic nitrate reduction on  $\text{TiO}_2$  nanoarrays for ammonia production and energy supply with zinc-nitrate batteries, *Energy Environ. Sci.*, 2021, **14**, 3938–3944.

45 X. Fan, C. Ma, D. Zhao, Z. Deng, L. Zhang, Y. Wang, Y. Luo, D. Zheng, T. Li, J. Zhang, S. Sun, Q. Liu and X. Sun, Unveiling selective nitrate reduction to ammonia with  $\text{Co}_3\text{O}_4$  nanosheets/ $\text{TiO}_2$  nanobelt heterostructure catalyst, *J. Colloid Interface Sci.*, 2023, **630**, 714–720.